Modification of hydrous ferric oxide by chitosan to enhance its adsorption performance toward perfluorooctane sulfonate

Ji Zang[a,†], Yuting He[a,†], Zhengjie Chen[a], Zhengxin Xie[a], Shisuo Fan[a,*], Jun Tang[b,*]

[a]*School of Resource and Environment, Anhui Agricultural University, Hefei 230036, China, Tel./Fax: +86551 65786790;*
emails: fanshisuo@ahau.edu.cn (S. Fan), 872579012@qq.com (J. Zang), 782247714@qq.com (Y. He), xiezx@ahau.edu.cn (Z. Xie)
[b]*Hefei Scientific Observing and Experimental Station of Agro-Environment, Ministry of Agriculture, P.R. China,*
Tel./Fax: +86551 65786790; email: tj2192@ahau.edu.cn/tangjun@ahau.edu.cn (J. Tang)

ABSTRACT

The aquatic environment is the main sink for perfluorooctane sulfonate (PFOS) accumulation, which is a typical persistent organic pollutant with high toxicity. In this study, a novel modification method was developed to prepare chitosan-modified hydrous ferric oxide (HFO), and then the adsorbent was used to remove PFOS from aqueous solution. The results found that the suitable added amount of chitosan for HFO modification was 8%. The influence of chitosan modification on HFO was characterized using scanning electron microscopy, Brunauer–Emmett–Teller, zeta potential, X-ray diffraction, Fourier-transform infrared spectroscopy, and X-ray photoelectron spectroscopy analysis. Chitosan modification could introduce functional groups on HFO, change its surface charge, and reduce its surface area. The pseudo-second-order kinetic model and Freundlich model could best describe the adsorption process of PFOS on 8%C-mHFO. The maximum adsorption capacity of PFOS on 8%C-mHFO reached 221.6 mg g^{-1}. The adsorption capacity gradually decreased with the increase of pH. Furthermore, coexisting anions and organic acids also reduced PFOS adsorption on 8%C-mHFO. Hydrophobic interaction, hydrogen bonding, ion-exchange, and electrostatic attraction may jointly play important roles in PFOS removal. Therefore, chitosan-modified HFO has the potential to remove PFOS from an aquatic environment.

Keywords: Hydrous ferric oxide; Chitosan; Perfluorooctane sulfonate; Characterization; Adsorption mechanisms

1. Introduction

Perfluorinated compounds (PFCs), as stable fluoro-surfactants, have attracted much attention in water bodies due to their persistence, toxicity, and bioaccumulation [1]. Perfluorooctane sulfonate (PFOS) is one of a class of industrial chemicals known as perfluoroalkyl acids, which have been widely used in food paper packaging, carpet surface protection, firefighting foam, and in the semiconductor industry [2]. PFOS shows both hydrophobic and hydrophilic properties owing to the C-F chain and sulfonate head group, which make PFOS being more soluble in aquatic solution than traditional hydrophobic pollutants [3,4]. PFOS pollution to varying degrees has been found in several water bodies, such as surface water, groundwater, and drinking water. The widespread appearance of PFOS poses great potential harm to human health and the ecological environment [5]. Thus, the removal of PFOS from aquatic environments has received much attention.

Many strategies have been adopted to remove PFCs from water effectively, involving adsorption [6], membrane filtration [7], sonochemical pyrolysis [8], and advanced oxidation [9]. Among them, adsorption is a feasible technology due to its simple operation, low environmental impact, high

* Corresponding authors.

† These authors contributed equally to this paper.

removal efficiency, and low cost. Many adsorbents, such as activated carbon [10–12], carbon nanotubes [13], organic polymers [14,15], and boehmite [16], metal oxidants [3], and biochar [17–19], have been widely investigated in previous studies. However, the application of most adsorbents was restricted by its high cost or low sorption capacities. Therefore, the preparation of a highly efficient and low-cost adsorbent is still in demand.

Hydrous ferric oxide (HFO) is a ubiquitous substance in aquatic ecosystems, which is widely distributed and has a high sorption capacity to pollutant in aquatic environment. In addition, HFO has been used as a cost-efficient and environmentally friendly adsorbent to remove pollutants in wastewater, such as tetracycline, phosphate, and arsenate [20–22]. As an effective adsorbent, HFO has received extensive attention in water pollution control [20,23]. To enhance the adsorption effect further, modification of HFO can be used to increase its specific properties, such as functional groups and surface charge. Therefore, the selection of modification method is crucial.

Chitosan is among one of the most important and most studied natural polymers due to its cationic nature, biocompatible, biodegradable as well as having adsorptive properties, therefore, it exhibits important potential application in wastewater treatment [24–26]. Chitosan is regarded as a good modifying agent since it contains amino groups and hydroxyl groups, and the polyanion properties determining it can bind anions in water treatment [27,28]. Further, chitosan modification increases the mechanical stability as well as providing more binding sites onto the surface of the matrix [29]. Previous studies have shown that chitosan-modified adsorbent can be used for the removal of different types of pollutants (i.e., dye wastewater, heavy metals, As(III), and phosphate anions) from aqueous solutions [27,29–34] Therefore, chitosan modification onto HFO can be a suitable choice, and the composite can be used as an adsorbent for the removal of PFOS. However, the influence of chitosan modification on the properties of HFO is still unclear and the adsorption mechanism needs further exploration.

In this study, a chitosan-modified hydrous ferric oxide (C-mHFO) composite material was synthesized and was used to remove PFOS from an aquatic environment. The aims of this study were (1) to investigate the effect of chitosan modification on the properties of HFO, (2) to study the adsorption performance of PFOS on C-mHFO, and (3) to reveal the adsorption mechanisms of PFOS on C-mHFO. Therefore, this study explored a novel modification method on HFO, which provided a reference for the removal of PFOS.

2. Materials and methods

2.1. Materials

PFOS (≥98% purity) was provided by MAYA Reagent (Zhejiang, China) and Pansine Chemical Co., Ltd. Analytical grade chitosan (>80% degree of deacetylation), sodium hydroxide, ammonium acetate, hydrochloric acid, and ferric chloride hexahydrate ($FeCl_3 \cdot 6H_2O$) were purchased from National Reagents Group (Shanghai, China, P.R.). Chromatographically pure acetonitrile and methanol were obtained from Tedia (Tedia, USA).

2.2. Preparation of chitosan-modified HFO

The C-mHFO composite material was prepared by dispersing 0, 0.2, 0.4, 0.6, 0.8, and 1 g of chitosan into 4% aqueous acetic acid solution (100 mL) and then 10 g of $FeCl_3 \cdot 6H_2O$ was added and stirred for 1 h until the mixture was completely homogeneous [35]. During continuous stirring, NaOH solution was slowly added to the above-mixture solution until reaching pH 7–8 to form a red-brown precipitate. The prepared suspension was kept at room temperature for 24 h to form the C-mHFO. The obtained C-mHFO particles were separated by centrifuging and then washed with ultrapure Milli-Q water several times. Finally, the wet solid C-mHFO was freeze-dried, and then manually milled, sieved through a 0.075 mm mesh to obtain a uniform powder, and stored in a brown glass bottle for further study. The 0%C-mHFO, 2%C-mHFO, 4%C-mHFO, 6%C-mHFO, 8%C-mHFO, and 10%C-mHFO denote 0%, 2%, 4%, 6%, 8%, and 10%, respectively, as the theoretical chitosan percentage in the composite.

2.3. Characterization of chitosan-modified HFO

A scanning electron microscope (FEI Q45, USA) was used to observe the HFO surface morphology. The mineral composition and type were confirmed using X-ray diffraction (Bruker D8 Advance, Germany) analysis. Fourier-transform infrared spectroscopy (FTIR) (Nicolette is50, Thermo Fisher Scientific, NY, USA) was used to characterize the functional groups in these samples within a wavenumber range from 4,000 to 400 cm^{-1}. X-ray photoelectron spectroscopy (XPS) was measured using a Thermo ESCALAB 250 (Thermo-VG Scientific, USA) spectrometer. The specific surface area of the C-mHFO was analyzed by a surface area and porosity analyzer (Micromeritics, Tristar II 3020, USA). zeta potentials of HFOs in the same electrolyte solution and concentration as in diameter monitoring using dynamic light scattering were measured with a zeta potential analyzer (ZetaPALS, Brookhaven, USA).

2.4. Sorption experiments

A 5,000 mg L^{-1} PFOS methanol stock solution was prepared, and then was diluted to the desired concentration for the adsorption experiments. A mass of 5 mg HFO or mHFO was added to 50 mL solutions of PFOS (PFOS = 5 mg L^{-1}, pH = 6.0). All experiments were performed under mechanical stirring with a speed of 150 rpm under darkness at 25°C.

The initial pH values of the PFOS solution were adjusted to 3–11 using 0.1 mol L^{-1} NaOH or 0.1 mol L^{-1} HCl. Adsorption kinetics experiments were carried out at pH = 6 with PFOS initial concentration of 5, 7.5, and 10 mg L^{-1}. Samples were collected at different time intervals. Adsorption isotherm experiments were performed with PFOS concentration ranging from 1 to 50 mg L^{-1}.

The PFOS amount adsorbed and removal efficiency were obtained based on Eqs. (1) and (2), respectively.

$$\text{Adsorption amount } \left(\text{mg·g}^{-1}\right) = \left(C_0 - C_e\right) \times \left(\frac{V}{m}\right) \qquad (1)$$

$$\text{Removal efficiency} \ (\%) = \frac{(C_0 - C_e)}{C_0} \times 100\% \qquad (2)$$

where C_0 is the initial PFOS concentration (mg L^{-1}), C_e is the equilibrium PFOS concentration (mg L^{-1}), V is the volume of PFOS solution (L), and m is the weight of adsorbent (g).

Each group of the above-experiments was done in triplicate and values averaged to account for experimental reproducibility.

2.5. Measurement of PFOS in solution

After the adsorption experiments, all tubes were centrifuged at 10,000 rpm for 10 min, and the supernatant was filtered with a 0.22 µm filter membrane, 0.5 mL of PFOS solution taken from the supernatant was diluted with 0.5 mL water containing 50% methanol (v/v = 1:1). PFOS in solution was analyzed using a Waters Acquity™ ultra performance liquid chromatography-tandem mass spectrometry (UPLC-MS/MS) system after sample treatment. Electrospray parameters in the negative ionization mode were set as follows: capillary voltage 2.0 kV, cone voltage 30 V, source temperature 150°C, desolvation temperature (N$_2$) 350°C, cone gas flow (N$_2$) 50 L h^{-1}, and desolvation gas flow (N$_2$) 700 L h^{-1}. Methanol containing 1‰ formic acid and water containing 5 mM ammonium acetate were used as the mobile phases B and A, respectively. The mobile phase had a flow rate of 0.3 mL min^{-1} and a 10 µL sample was injected for PFOS detection in the UPLC-MS/MS system with the temperature of the column controlled at around 40°C ± 2°C. The gradient program lasted for 5 min. Mobile phase "A" was set to 60%, 60%, 10%, 10%, 60%, and 60% at 0, 0.2, 2, 3, 3.1, and 5 min, respectively.

2.6. Model fitting

To investigate the adsorption kinetics of PFOS adsorption on HFO (including 0%C-mHFO and 8%C-mHFO), pseudo-first-order and pseudo-second-order models (Eqs. (3) and (4), respectively) were used to fit the adsorption kinetics process.

The linear expression of the pseudo-first-order equation is described as [36]:

$$q_t = q_e\left(1 - \exp(-k_1 t)\right) \qquad (3)$$

The linear expression of the pseudo-second-order equation is described as [37]:

$$q_t = \frac{k_2 q_e^2 t}{\left(1 + k_2 q_e t\right)} \qquad (4)$$

where q_t (mg g^{-1}) and q_e (mg g^{-1}) are the adsorption amount at time t and equilibrium amount, respectively. k_1 (min^{-1}) and k_2 (g (mg min)$^{-1}$) represent the reaction rate constants of pseudo-first-order and pseudo-second-order models, respectively.

To describe the adsorption isotherm process of PFOS solution onto HFO (including 0%C-mHFO and 8%C-mHFO), Langmuir and Freundlich models (Eqs. (5) and (6),

respectively) were examined to describe the adsorption process.

The Langmuir adsorption isotherm is described as [38]:

$$q_e = \frac{q_m K_L C_e}{\left(1 + K_L C_e\right)} \qquad (5)$$

The Freundlich adsorption isotherm is described as [39]:

$$q_e = K_F C_e^{1/n} \qquad (6)$$

where q_e (mg g^{-1}) is the equilibrium adsorption capacity and q_m (mg g^{-1}) is the maximum adsorption capacity. K_F and K_L (L mg^{-1}) are the Freundlich and Langmuir adsorption isotherm constants, respectively; $1/n$ is the adsorption affinity constant.

3. Results and discussion

3.1. Effect of chitosan amount on PFOS adsorption and surface area change

The effects of adding various amounts of chitosan in the HFO composite (0%, 2%, 4%, 6%, 8%, and 10%, wt.%) on the removal efficiency of PFOS and the change of surface area are shown in Fig. 1. The adsorption capacity of the PFOS increased with the increasing amount of chitosan in the adsorbent over the range of 0% to 8%. However, as the chitosan amount increased to a value of 10%, the adsorption capacity of PFOS on HFO decreased, which was mainly because the surface of HFO was saturated by chitosan molecules at the 8% loading level and that further increasing the amount of chitosan mixed with the HFO did not lead to higher surface coverage [40]. 8%C-mHFO exhibited the highest adsorption capacity. The 8% chitosan content in the modified adsorbent increased adsorption capacity for PFOS by 35%. The specific surface area of HFO decreased with the increase of chitosan amount since the pore structure may be blocked. Therefore, the 8%C-mHFO adsorbent was assumed optimal for the preparation of modified adsorbent and was used for adsorptive removal of PFOS in the subsequent experiments.

3.2. Characterization of HFO

scanning electron microscopy (SEM) images of 0%C-mHFO and 8%C-mHFO with different magnifications are displayed in Fig. 2. It can be seen that 8%C-mHFO had some irregularly shaped granules and micropores in the matrix and very rough microstructure. However, the surface of 0%C-mHFO was quite smooth, indicating that the chitosan was successfully attached to the surfaces. The surface of 8%C-mHFO was much rougher than the HFO (Fig. 2g), which may provide additional adsorption sites for PFOS, thus increasing the adsorption capacity of HFO.

X-ray diffraction (XRD) was used to analyze the crystal structure of the material [41,42]. Fig. 3a shows the XRD spectra of 0%C-mHFO and 8%C-mHFO; the peak shapes of 0%C-mHFO and 8%C-mHFO in the range of 20°–60° (2θ) were not sharp, and these peaks were similar to ferrihydrite [43]. The XRD pattern indicated that 0%C-mHFO and
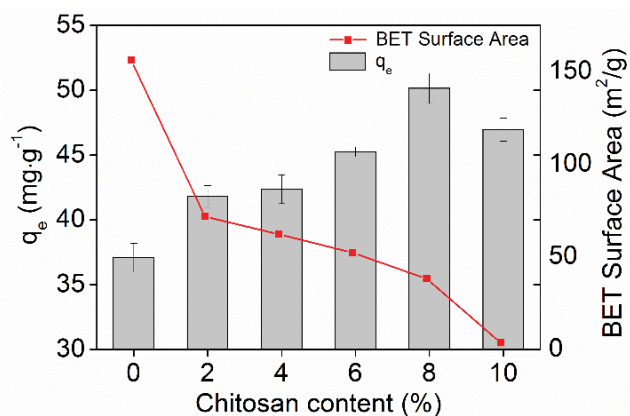
Fig. 1. Adsorptive removal of PFOS on the hydrous ferric oxide of different chitosan amount (adsorption time = 4 h; initial concentration of PFOS = 5 mg L^{-1}; adsorbent dose = 0.1 g L^{-1}; rotating speed = 150 rpm; temperature = 25°C).

8%C-mHFO showed one broad peak at 35.2°, suggesting that the synthesized HFO used in this study was an amorphous HFO with poor crystallinity.

The zeta potentials of 0%C-mHFO and 8%C-mHFO are listed in Fig. 3b. The 0%C-mHFO shows typical amphoteric nature with an isoelectric point of about 6.7, whereas 8%C-mHFO had a positive surface charge at pH lower than 9.64 due to the presence of amino groups on the surface [44]. Thus, chitosan modification significantly influenced the surface charge of HFO, which may affect the removal of PFOS.

FTIR spectra of 0%C-mHFO, 8%C-mHFO, and 8%C-mHFO + PFOS are shown in Fig. 4 and specific functional groups are listed in Table 1. To understand better the role of chitosan-enhancement on the removal of PFOS by HFO, the differences in functional groups of 8%C-mHFO before and after adsorption with PFOS were analyzed using FTIR spectroscopy. After the HFO was modified with chitosan, new characteristic peaks at 895 cm^{-1} (C–H deformation of β-1,4 glycosidic linkage) and 1,069 cm^{-1} (skeletal vibration
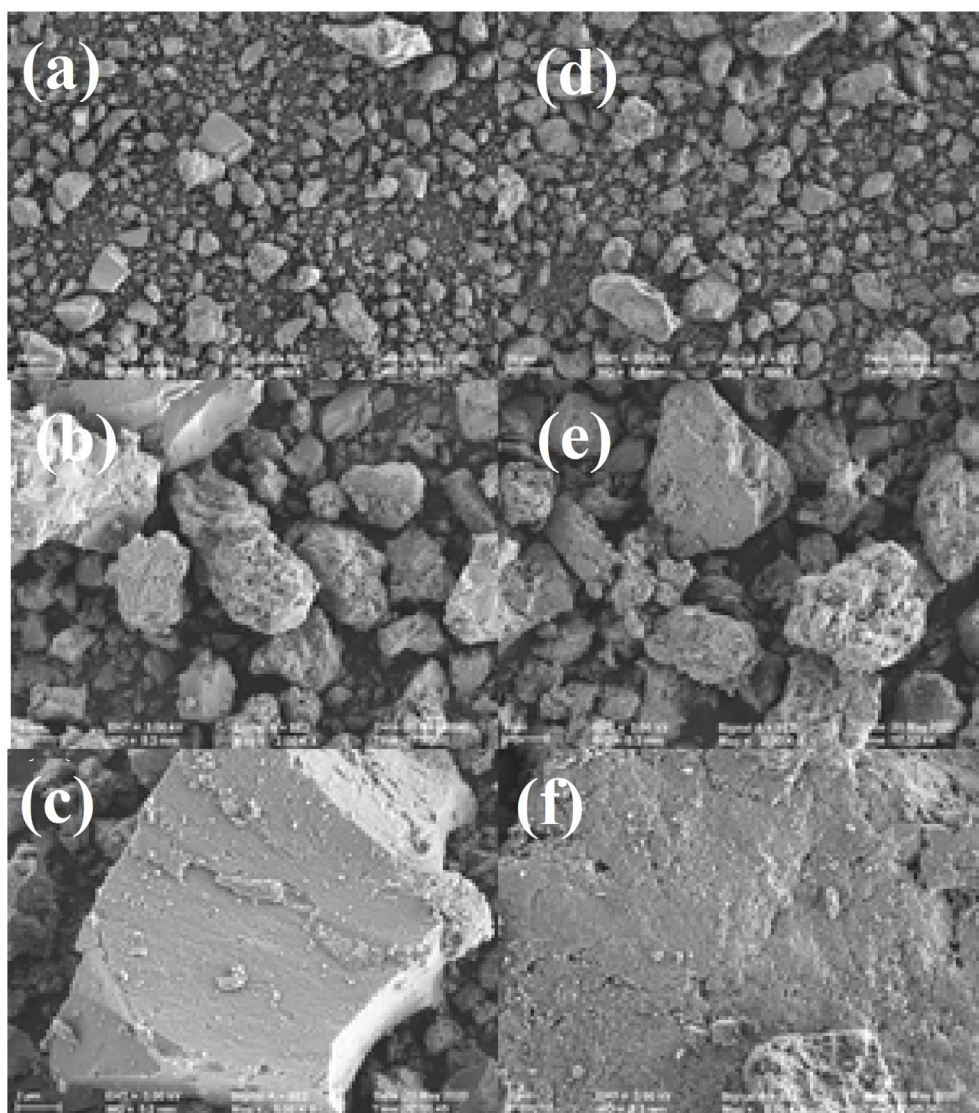
Fig. 2. SEM of 0%C-mHFO (a–c) and 8%C-mHFO (d–f) with different magnifications.
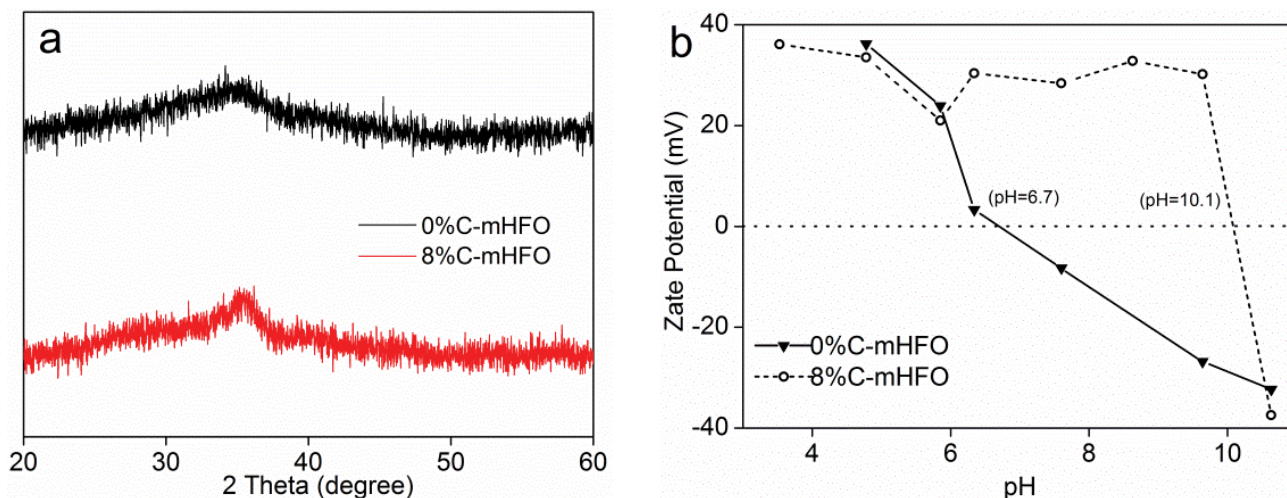
Fig. 3. XRD patterns of 0%C-mHFO and 8%C-mHFO (a), zeta potential of 0%C-mHFO and 8%C-mHFO (b).

involving the bridge C–O stretch) were observed in Fig. 4b, which were characteristic peaks of chitosan. The above-mentioned analysis clearly indicated that HFO was successfully modified with chitosan [45–48]. The FTIR spectra of 8%C-mHFO after PFOS adsorption is shown in Fig. 4c. The peak at 1,024 cm^{-1} attributed to O–H vibration disappeared after the sorption of the PFOS on the 8%C-mHFO [49]. This strongly suggested that the sorption of PFOS on 8%C-mHFO involved ion-exchange between PFOS and the OH$^-$, and the OH$^-$ may be replaced by PFOS$^-$. For PFOS adsorbed on 8%C-mHFO, the new bands at 1,242; 1,205 and 1,401 cm^{-1} were ascribed to CF$_2$, CF$_3$, and carboxylate groups, respectively [50,51]. This provided evidence for the successful adsorption of PFOS on 8%C-mHFO. After the adsorptive reaction, the peak of 8%C-mHFO at 3,417 cm^{-1} (attributed to O–H stretching) shifted to 3,405 and 1,336 cm^{-1} (attributed to C–H bending) disappeared [52], which implied the chemical interaction of adsorbents with PFOS molecules. The C–H groups on chitosan can develop relatively weak ion-dipole interactions with the S–O groups of PFOS [53]. Bands at 1,067 cm^{-1} corresponded to C–O stretching for the glucosamine residue, these groups procured the adsorption of PFOS by the distribution of its hydrophobic C–F chains over the biochar hydrophobic regions [54,55]. In contrast, the bands at 3,417 cm^{-1} corresponded to O–H groups, which could develop relatively weak hydrophilic force interactions with the S–OH groups of PFOS.

XPS spectra of HFO are shown in Fig. 5 and the elements Fe 2p, N 1s, O 1s, and F 1s could be observed on the surface of HFO (Fig. 5a–c). According to the XPS spectra of 0%C-mHFO and 8%C-mHFO, the relative percentage of elements on the surfaces of the original, chitosan-loaded HFO samples were determined, and the results are listed in Table 2. From Table 2, after modification with chitosan, the relative percentage of N content greatly increased from 0.14% to 2.59%, indicating that the chitosan was successfully grafted on the surfaces of HFO. The presence of F 1s in 8%C-mHFO after PFOS adsorption confirmed that PFOS had been adsorbed on the surface of 8%C-mHFO (Fig. 5h).
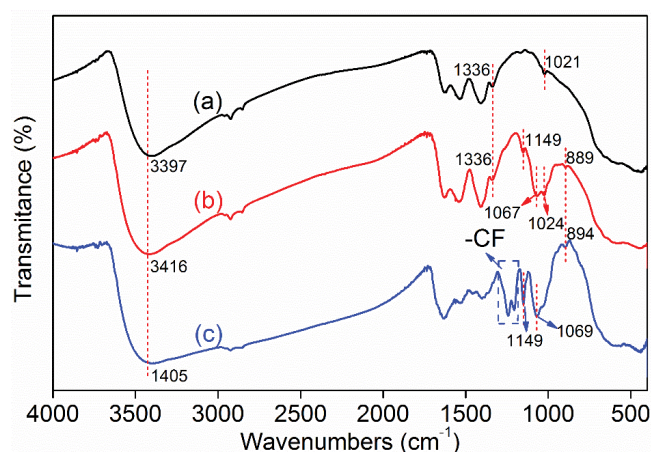
Fig. 4. FTIR spectra of 0%C-mHFO (a), 8%C-mHFO (b) and 8%C-mHFO + PFOS (c).

The surface O 1s spectra of 8%C-mHFO before and after PFOS adsorption were analyzed by XPS peak differentiating, and are demonstrated in Fig. 5d and f. Fig. 5d shows that the O 1s core-level spectrum could be decomposed into three peaks at 530.09, 531.56, and 532.98 eV, which were assigned to Fe–O, –OH, and C–O, respectively. After PFOS adsorption, the relative percentage of O 1s content greatly decreased from 39.11% to 30.56%, whereas that of –OH reduced from 34.15% to 22.52%. This result indicated that the decrease in O element was mainly ascribed to the ion-exchange between PFOS and –OH [56], which is in accordance with the results of FTIR studies.

The N 1s core-level spectra before and after PFOS adsorption are explained in Fig. 5c and g. For the 8%C-mHFO before sorption, the binding energies at 399.61 and 401.89 eV were attributed to the nitrogen in the –NH/NH$_2$ and –NH$_3^+$ [57]. After the sorption of PFOS on the 8%C-mHFO, the peaks belonging to the protonated nitrogen atom (NH$_3^+$) on the 8%C-mHFO increased distinctly, the percentage of NH$_3^+$ increased from 31.05% to 65.18%, signifying

Table 1
Functional groups of 0%C-mHFO, 8%C-mHFO and 8%C-mHFO + PFOS

0%C-mHFO (cm^{-1})	8%C-mHFO (cm^{-1})	8%C-mHFO + PFOS (cm^{-1})	Assignment
3,397	3,416	3,405	O–H stretching
1,629	1,629	1,630	Bending vibration of OH
	1,149	1,149	C–N stretching
1,336	1,336		C–H bending
		1,242	CF$_2$ and CF$_3$ groups
		1,205	CF$_2$ and CF$_3$ groups
	1,067	1,069	C–O stretching for glucosamine residue
1,021	1,024		–OH
	889	894	C–H deformation for β-1,4 glycosidic linkage
433	448	441	Fe–O

Table 2
Relative content of elements on the surface of 0%C-mHFO, 8%C-mHFO and 8%C-mHFO + PFOS

Element	0%C-mHFO (%)	8%C-mHFO (%)	8%C-mHFO + PFOS (%)
Fe 2p	7.75	9.79	7.51
N 1s	0.14	2.59	2.88
O 1s	45.04	39.11	30.56
F 1s	0.1	0.11	20.09

that the anionic PFOS were adsorbed on the protonated amine groups on the adsorbent surface via the electrostatic interaction. Similar results were obtained by Deng et al. [6].

3.3. Effect of initial solution pH

Solution pH is an important factor during the adsorption process, which can influence the speciation of pollutants and the surface charge of adsorbents. As shown in Fig. 6, the impact of initial solution pH on PFOS sorption exhibited a similar trend for 0%C-mHFO and 8%C-mHFO. The results showed that solution pH obviously influenced the PFOS removal efficiency. As the pH increased from 3.66 to 10.61, the adsorption quantity decreased significantly. Specifically, the adsorption performance decreased very slightly from pH 3.66 to pH 6.68, while it dropped much faster with the pH increase after pH 7.31. A similar solution pH effect has also been observed in previous reports for various adsorbents [56,58]. The pK$_a$ value of PFOS was –3.4 and PFOS showed a negative charge as a whole. This was because pH in the acidic region was conducive to the protonation of the adsorbent surface, which could enhance the electrostatic attraction between the adsorbent surface and the PFOS anions and promotes PFOS adsorption. This was because pH in the acidic region was conducive to the protonation of the adsorbent surface, which could enhance the electrostatic attraction between the adsorbent surface and the PFOS anions and promoted PFOS adsorption. However, the PFOS adsorption on the two adsorbents is a chemisorption-dominated process, and the adsorption from the electrostatic attraction is not a major contribution to this process. The PFOS adsorption performance of the two adsorbents just decreased very slightly from pH 3.66

to 6.68. The removal rate of PFOS decreased significantly at pH > 7.31 due to the occurrence of electrostatic repulsion.

3.4. Effect of organic acid and coexisting anions

The presence of organic acid and coexisting anions in solution can affect the PFOS adsorption on HFO. Organic acid and coexisting anions involved Cl$^-$, SO$_4^{2-}$, NO$_3^-$, L-malic acid (L-MA), citric acid (CA), and oxalic acid (OX). Fig. 7 depicts the adsorption capacity of PFOS (5 mg L^{-1}) in the presence of the other competitive anions and organic acids (20 mg L^{-1}) at room temperature. The PFOS adsorption capacity significantly decreased in the presence of competing anions and organic acid due to saturation of the limited sites on the surface of HFO. The anionic Cl$^-$ had almost no effect on the adsorption of PFOS by 8%C-mHFO, while the organic acids had significant effects on PFOS removal, and the 0%C-mHFO hardly showed removal effect for PFOS in the presence of 20 mg L^{-1} OX. The adsorption capacity was significantly lower in the case of the binary solute systems PFOS + SO$_4^{2-}$ than with a single solute system, and this could be explained by the competition of PFOS with SO$_4^{2-}$ ions and the larger ionic radius than the other anions chosen in this study [59]. The aforementioned observations indicated that the synthesized 8%C-mHFO had better adsorption of PFOS than 0%C-mHFO even in the presence of other inorganic anions and organic acids when used for water treatment.

3.5. Adsorption kinetics

The adsorption kinetics curves are shown in Fig. 8. The adsorption process exhibited the same trend, namely,
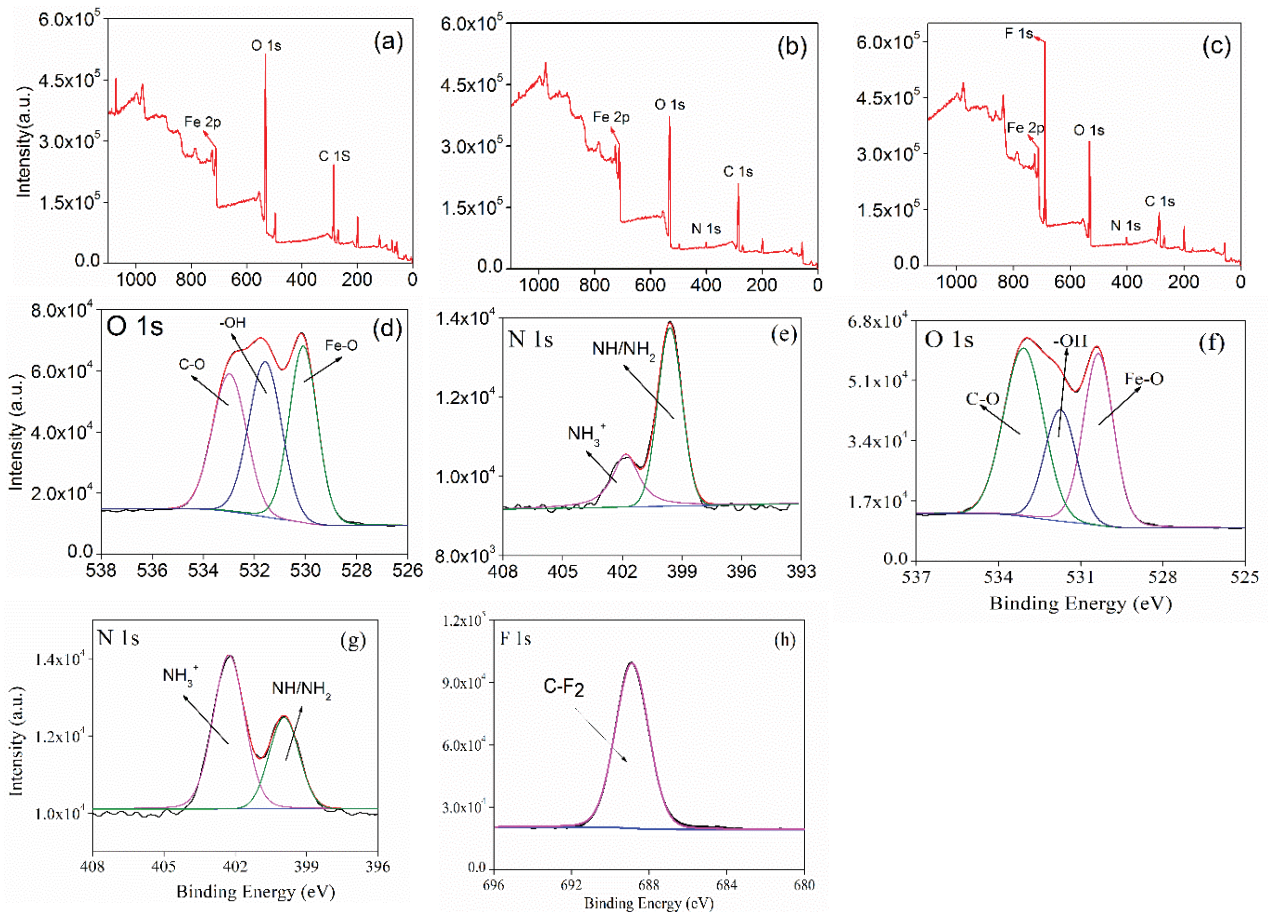
Fig. 5. XPS survey scan of (a) 0%C-mHFO, (b) 8%C-mHFO and (c) 8%C-mHFO + PFOS, and XPS analysis of (d) O 1s, (e) N 1s for 8%C-mHFO, (f) O 1s, (g) N 1s, and (h) F 1s for PFOS adsorption on 8%C-mHFO.

that adsorption proceeded quickly in the first 3 h. As the active sites on the adsorbent were gradually occupied, the adsorption rate became slower, a similar trend was also reported by other studies [60,61]. The fitting parameters are listed in Table 3. The coefficient of determination (R^2) of the HFO adsorbent suggested that the pseudo-second-order model better fitted the experimental data than the pseudo-first-order model, suggesting that the chemical adsorption was mainly controlled by the adsorption rate which involved valency forces through sharing or exchanging electrons between the 8%C-mHFO and PFOS [62]. Besides, 8%C-mHFO exhibited a better adsorption capacity than 0%C-mHFO. This behavior was attributed to the modification of HFO by chitosan to increase various functional groups (including –NH$_2$ and –OH), thus there existed electrostatic adsorption sites and chemical adsorption sites for the sorption of PFOS by electrostatic adsorption and chemical adsorption. This is consistent with the results found from FTIR and XPS. The kinetics study showed that 4 h was sufficient for adsorption completion. It is commonly considered that the hydrogen bond between the sulfonate groups in PFOS molecules and amino, hydroxyl groups on the 8%C-mHFO surface as well as the electrostatic interaction are responsible for the fast sorption of PFOS and equilibrium may be reached in a short period [6,53].
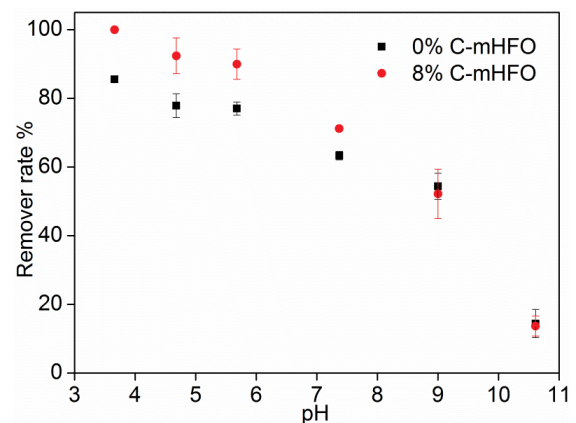
Fig. 6. Effect of pH on PFOS adsorption on 0%C-mHFO and 8%C-mHFO (adsorption time = 4 h; initial concentration of PFOS = 5 mg L^{-1}; adsorbent dose = 0.1 g L^{-1}; rotating speed = 150 rpm; temperature = 25°C).

3.6. Adsorption isotherms

Fig. 9 illustrates the adsorption isotherms of PFOS on 0%C-mHFO and 8%C-mHFO. The obtained parameters are listed in Table 4. The results showed that the PFOS adsorption

behaviors by 0%C-mHFO and 8%C-mHFO were different. The coefficient of determination (R^2) for the Freundlich model was higher than that for the Langmuir model for 8%C-mHFO adsorption isotherms. This could be due to the
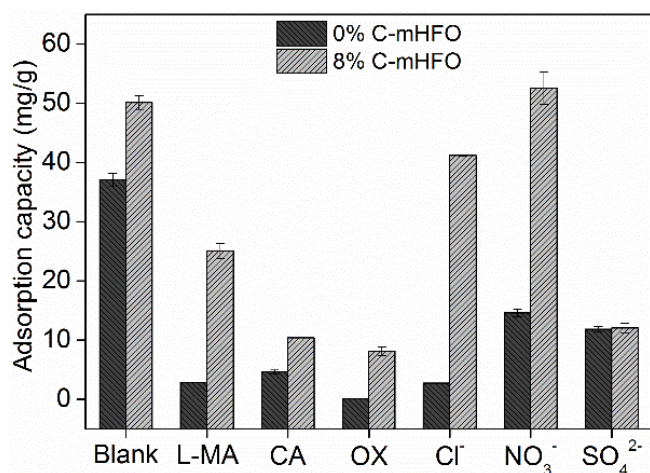
Fig. 7. Effect of coexisting anions and organic acid on PFOS adsorption on 0%C-mHFO and 8%C-mHFO (adsorption time = 4 h; initial concentration of PFOS = 5 mg L^{-1}; adsorbent dose = 0.1 g L^{-1}; rotating speed = 150 rpm; temperature = 25°C).

introduction of amino groups with higher affinity for PFOS and the uptakes occurred by multilayer adsorption [55]. However, for 0%C-mHFO adsorbent, the Langmuir model fit the data better, showing possible monolayer sorption. Thus, it can be concluded that the adsorption mechanisms were different for the two different adsorbents.

As can be seen from Table 4, according to the Langmuir fitting, the maximum adsorption capacity of PFOS on the 8%C-mHFO was 221.6 mg g^{-1}, which was 1.67 times that of 0%C-mHFO. The higher adsorption capacity for the adsorption of PFOS on 8%C-mHFO may be due to the higher content of –OH, –NH$_2$, and C–H groups present in this adsorbent. The K_L of 8%C-mHFO was larger than that of 0%C-mHFO, suggesting the high affinity of 8%C-mHFO to PFOS. Furthermore, the factor "1/n" gave an indication of the favorability of adsorption. Values of 1/n smaller than 0.5 represented that the adsorbate was easily adsorbed; values of 1/n larger than 2 indicated the adsorbate was hardly adsorbed [63]. In this study, the values of 1/n obtained (around 0.5164 and 0.2647 for 0%C-mHFO and 8%C-mHFO, respectively) indicated that C-mHFO was favorable to the adsorption process. Moreover, the value of 1/n from the Freundlich model indicated the surface properties of the adsorbents. If the values were close to 1, it indicated a homogeneous surface [53]. However, the 1/n value of 8%C-mHFO was lower than the 0%C-mHFO

Table 3
Fitting parameters of adsorption kinetic of PFOS on HFO

Adsorben+ts	Concentration (mg L^{-1})	Pseudo-first-order equation			Pseudo-second-order equation		
		k_1 (min^{-1})	q_e (mg g^{-1})	R^2	k_2 (g mg^{-1} min^{-1})	q_e (mg g^{-1})	R^2
0%C-mHFO	5	0.04120	25.19	0.9592	2.500×10^{-3}	26.80	0.9947
	7.5	0.04570	27.17	0.8881	2.500×10^{-3}	28.90	0.9296
	10	0.03520	34.78	0.9623	1.400×10^{-3}	37.59	0.9338
8%C-mHFO	5	0.04050	40.64	0.9347	1.500×10^{-3}	43.30	0.9983
	7.5	0.02920	69.59	0.9677	5.467×10^{-4}	76.48	0.9949
	10	0.02850	94.35	0.9484	3.793×10^{-4}	103.79	0.9964
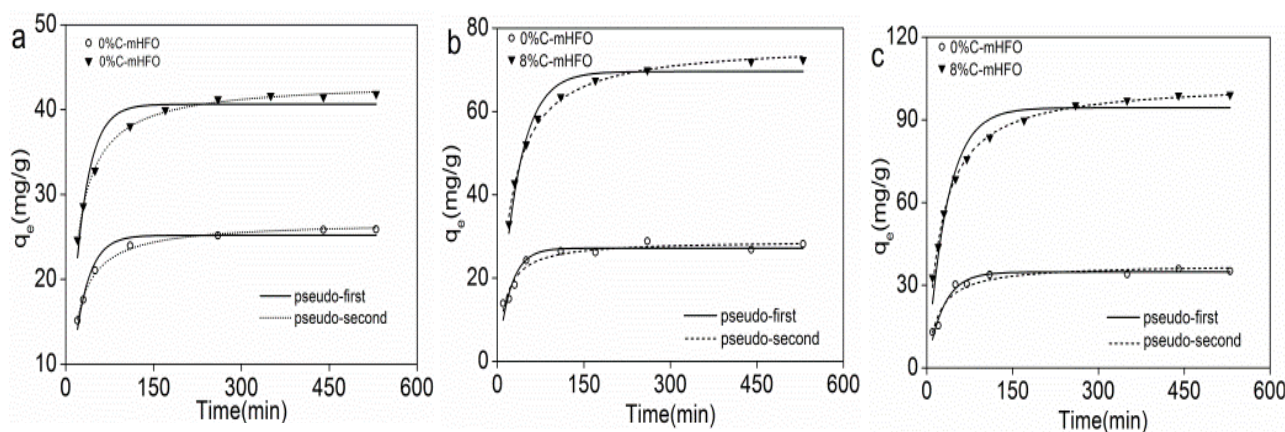
Fig. 8. Kinetic fits for PFOS adsorption on hydrous ferric oxide (25°C) using different kinetic models: (a) initial concentration = 5 ppm, (b) initial concentration = 7.5 ppm, (c) initial concentration = 10 ppm (adsorption time = 4 h; adsorbent dose = 0.1 g L^{-1}; rotating speed = 150 rpm; temperature = 25°C).

Table 4
Adsorption isotherm parameters of PFOS sorption onto the adsorbents

Adsorbents	Freundlich			Langmuir		
	K_F	$1/n$	R^2	q_m (mg g^{-1})	K_L (L mg^{-1})	R^2
0%C-mHFO	15.23	0.5164	0.9786	132.5	0.07080	0.9939
8%C-mHFO	102.3	0.2647	0.9902	221.6	1.047	0.8682

Table 5
Comparison of different adsorbents in the removal of PFOS based on adsorption capacity

Adsorbent	Adsorption capacity (mg g^{-1})	Reference
Alumina	0.02200	[61]
Boehmite	0.2630	[16]
AC-H$_3$PO$_4$	75.13	[10]
Activated carbon	138.0	[12]
Corn straw-derived biochar	169.3	[54]
Sawdust and red mud derived biochar	194.6	[53]
Polyaniline nanotubes	1651	[14]
8%C-mHFO	221.6	Present study

value, indicating heterogeneity of the 8%C-mHFO, which was further confirmed by the SEM image Fig. 2.

3.7. Comparison of the 8%C-mHFO adsorbent with previous adsorbents

The maximum adsorption capacity obtained in this research was compared with previous adsorbents. As shown in Table 5, the adsorbent used in this study showed environmental friendliness, higher adsorption capacity, and cost-effectiveness compared with other adsorbents. Thus, the adoption of C-mHFO for the preparation of adsorbent for PFOS removal from aqueous solutions showed promise.

3.8. Adsorbent regeneration study

Reusability property is an important factor to assess the practical application of adsorbents. A regeneration study of 8%C-mHFO is shown in Fig. 10. After the first run

of PFOS, the spent materials were collected and washed several times with 1 M ethanol, which was used as an elution agent to rinse the adsorbed PFOS molecules from the surface of the materials. Then, the materials were dried in vacuum for the first regeneration cycle. The adsorption density of 8%C-mHFO slightly decreased in the second and third cycles, which could be explained by more adsorption sites being occupied after more cycles of reuse. The results indicated that 8%C-mHFO possessed sufficient chemical stability for reuse after three cycles and had practical application potential.

3.9. Adsorption mechanisms of PFOS onto 8%C-mHFO

According to the results of adsorption kinetics of 8%C-mHFO (as shown in Fig. 8), the adsorption process involved physical action and chemical bonding (electrostatic interaction, ion-exchange, chemical action, also hydrogen bonding). According to FTIR analysis (as shown
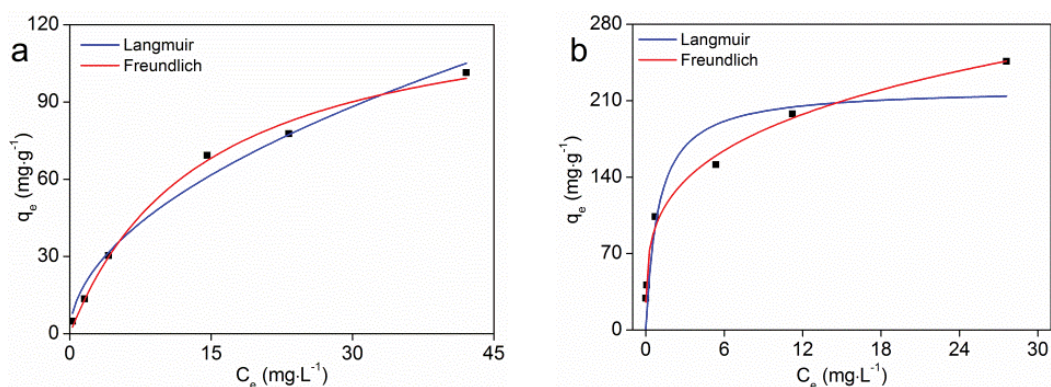
Fig. 9. Adsorption isotherm models fitting for PFOS adsorption onto 0%C-mHFO (a) and 8%C-mHFO (b).

in Fig. 4) and XPS analysis (as shown in Fig. 5), surface complexation played an important role during the adsorption between PFOS and 8%C-mHFO, including hydrogen bonding and electronic attraction. –OH and –NH$_2$ functional groups were likely to participate in PFOS binding. The O–H disappears after the sorption of the PFOS on the 8%C-mHFO, indicating that the mechanism referred to ion-exchange between 8%C-mHFO and PFOS. Furthermore, hydrophobic interaction was an important mechanism involved in PFOS adsorption onto 8%C-mHFO. In summary, a schematic diagram of adsorption mechanisms of PFOS on 8%C-mHFO is presented in Fig. 11.

4. Conclusions

FTIR and XPS analysis confirmed that 8% (w/w) C-mHFO significantly increased the content of –NH$_2$ and –OH functional groups, which was beneficial for PFOS adsorption. The adsorption of PFOS on the HFO samples decreased as pH value increased. The pseudo-second-order model and Freundlich model better described the adsorption performance of PFOS on 8%C-mHFO. The maximum adsorption capacity of the 8%C-mHFO toward PFOS reached

221.6 mg g^{-1}. Electrostatic interactions, hydrogen bonding, ion-exchange, and hydrophobic interaction were the main adsorption mechanisms between PFOS and 8%C-mHFO. Therefore, C-mHFO had a promising application in wastewater treatment for the removal of high or low concentrations of PFOS.
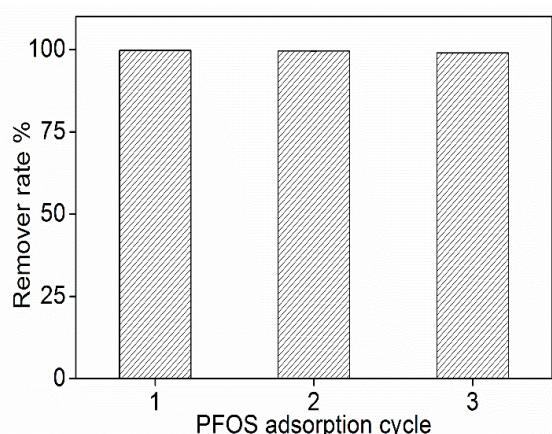
Fig. 10. Regeneration study of 8%C-mHFO.
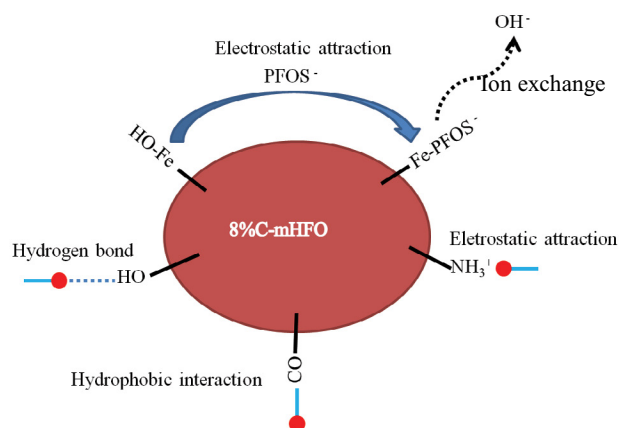
Fig. 11. Schematic diagram of adsorption mechanism of PFOS on 8%C-mHFO.

References

[1] K.S. Suh, E.M. Choi, Y.J. Kim, S.M. Hong, S.Y. Park, S.Y. Rhee, S. Oh, S.W. Kim, Y.K. Pak, W. Choe, S. Chon, Perfluorooctanoic acid induces oxidative damage and mitochondrial dysfunction in pancreatic β-cells, Mol. Med. Rep., 15 (2017) 3871–3878.
[2] D. Zhang, Q. Luo, B. Gao, S.-Y.D. Chiang, D. Woodward, Q. Huang, Sorption of perfluorooctanoic acid, perfluorooctane sulfonate and perfluoroheptanoic acid on granular activated carbon, Chemosphere, 144 (2016) 2336–2342.
[3] J.-N. Uwayezu, L.W.Y. Yeung, M. Bäckström, Sorption of PFOS isomers on goethite as a function of pH, dissolved organic matter (humic and fulvic acid) and sulfate, Chemosphere, 233 (2019) 896–904.
[4] S. Rayne, K. Forest, Perfluoroalkyl sulfonic and carboxylic acids: a critical review of physicochemical properties, levels and patterns in waters and wastewaters, and treatment methods, J. Environ. Sci. Health., Part A, Environ. Sci. Eng., 44 (2009) 1145–1199.
[5] X.-T. Chen, P.-F. Yu, L. Xiang, H.-M. Zhao, Y.-W. Li, H. Li, X.-Y. Zhang, Q.-Y. Cai, C.-H. Mo, M.H. Wong, Dynamics, thermodynamics, and mechanism of perfluorooctane sulfonate (PFOS) sorption to various soil particle-size fractions of paddy soil, Ecotoxicol. Environ. Saf., 206 (2020) 111105, doi: 10.1016/j.ecoenv.2020.111105.
[6] S. Deng, L. Niu, Y. Bei, B. Wang, J. Huang, G. Yu, Adsorption of perfluorinated compounds on aminated rice husk prepared by atom transfer radical polymerization, Chemosphere, 91 (2013) 124–130.
[7] C.Y. Tang, Q.S. Fu, A.P. Robertson, C.S. Criddle, J.O. Leckie, Use of reverse osmosis membranes to remove perfluorooctane sulfonate (PFOS) from semiconductor wastewater, Environ. Sci. Technol., 40 (2006) 7343–7349.
[8] M. Trojanowicz, A. Bojanowska-Czajka, I. Bartosiewicz, K. Kulisa, Advanced oxidation/reduction processes treatment for aqueous perfluorooctanoate (PFOA) and perfluorooctanesulfonate (PFOS) – a review of recent advances, Chem. Eng. J., 336 (2018) 170–199.
[9] A. Santos, S. Rodríguez, F. Pardo, A. Romero, Use of Fenton reagent combined with humic acids for the removal of PFOA from contaminated water, Sci. Total Environ., 563–564 (2016) 657–663.
[10] B.O. Fagbayigbo, B.O. Opeolu, O.S. Fatoki, T.A. Akenga, O.S. Olatunji, Removal of PFOA and PFOS from aqueous solutions using activated carbon produced from *Vitis vinifera* leaf litter, Environ. Sci. Pollut. Res., 24 (2017) 13107–13120.
[11] X. Chen, X. Xia, X. Wang, J. Qiao, H. Chen, A comparative study on sorption of perfluorooctane sulfonate (PFOS) by chars, ash and carbon nanotubes, Chemosphere, 83 (2011) 1313–1319.
[12] W. Wang, Z. Du, S. Deng, M. Vakili, L. Ren, P. Meng, A. Maimaiti, B. Wang, J. Huang, Y. Wang, G. Yu, Regeneration of PFOS loaded activated carbon by hot water and subsequent aeration enrichment of PFOS from eluent, Carbon, 134 (2018) 199–206.
[13] S. Deng, Q. Zhang, Y. Nie, H. Wei, B. Wang, J. Huang, G. Yu, B. Xing, Sorption mechanisms of perfluorinated compounds on carbon nanotubes, Environ. Pollut., 168 (2012) 138–144.

[14] C. Xu, H. Chen, F. Jiang, Adsorption of perflourooctane sulfonate (PFOS) and perfluorooctanoate (PFOA) on polyaniline nanotubes, Colloids Surf., A, 479 (2015) 60–67.

[15] Y. Gao, S. Deng, Z. Du, K. Liu, G. Yu, Adsorptive removal of emerging polyfluoroalky substances F-53B and PFOS by anion-exchange resin: a comparative study, J. Hazard. Mater., 323 (2017) 550–557.

[16] F. Wang, C. Liu, K. Shih, Adsorption behavior of perfluorooctanesulfonate (PFOS) and perfluorooctanoate (PFOA) on boehmite, Chemosphere, 89 (2012) 1009–1014.

[17] T. Feng, T. Yi, Q.B. Wang, P.W. Li, Shrimp shells-derived biochar for efficient adsorption of Pb^{2+} in aqueous solutions, Desal. Water Treat., 233 (2021) 106–117.

[18] J.M. Koroma, K.B. Pu, H. Zhang, J.R. Bai, M.S. Almouctar, Y.H. Wang, Methylene blue adsorption on *Parinari excelsa* biochar in aqueous solution, Desal. Water Treat., 233 (2021) 351–360.

[19] S. Chen, T. Wang, C. Chen, J.X. Liu, M. Mei, J.P. Xie, J.P. Li, Study on adsorption of Direct Red 23 by biochar derived from co-pyrolysis of sewage sludge and rice husk waste: optimization, isotherm, kinetic, thermodynamic and mechanisms, Desal. Water Treat., 221 (2021) 378–395.

[20] C. Gu, K.G. Karthikeyan, Interaction of tetracycline with aluminum and iron hydrous oxides, Environ. Sci. Technol., 39 (2005) 2660–2667.

[21] Z. Wang, Y. Lin, D. Wu, H. Kong, Hydrous iron oxide modified diatomite as an active filtration medium for phosphate capture, Chemosphere, 144 (2016) 1290–1298.

[22] L. Boukemara, C. Boukhalfa, Phosphate removal from aqueous solution by hydrous iron oxide freshly prepared effects of pH, iron concentration and competitive ions, Procedia Eng., 33 (2012) 163–167.

[23] J. Majzlan, Thermodynamic stabilization of hydrous ferric oxide by adsorption of phosphate and arsenate, Environ. Sci. Technol., 45 (2011) 4726–4732.

[24] X. Wu, M. Huang, T. Zhou, J. Mao, Recognizing removal of norfloxacin by novel magnetic molecular imprinted chitosan/γ-Fe_2O_3 composites: selective adsorption mechanisms, practical application and regeneration, Sep. Purif. Technol., 165 (2016) 92–100.

[25] R. Huang, Q. Liu, J. Huo, B. Yang, Adsorption of methyl orange onto protonated cross-linked chitosan, Arabian J. Chem., 10 (2017) 24–32.

[26] B. Tanhaei, A. Ayati, M. Lahtinen, M. Sillanpää, Preparation and characterization of a novel chitosan/Al_2O_3/magnetite nanoparticles composite adsorbent for kinetic, thermodynamic and isotherm studies of Methyl orange adsorption, Chem. Eng. J., 259 (2015) 1–10.

[27] U. Habiba, A.M. Afifi, A. Salleh, B.C. Ang, Chitosan/(polyvinyl alcohol)/zeolite electrospun composite nanofibrous membrane for adsorption of Cr^{6+}, Fe^{3+} and Ni^{2+}, J. Hazard. Mater., 322 (2017) 182–194.

[28] P.S. Bakshi, D. Selvakumar, K. Kadirvelu, N.S. Kumar, Chitosan as an environment friendly biomaterial – a review on recent modifications and applications, Int. J. Biol. Macromol., 150 (2020) 1072–1083.

[29] T.A. Saleh, A. Sarı, M. Tuzen, Chitosan-modified vermiculite for As(III) adsorption from aqueous solution: equilibrium, thermodynamic and kinetic studies, J. Mol. Liq., 219 (2016) 937–945.

[30] N. Caner, A. Sarı, M. Tüzen, Adsorption characteristics of mercury(II) ions from aqueous solution onto chitosan-coated diatomite, Ind. Eng. Chem. Res., 54 (2015) 7524–7533.

[31] X. Liu, L. Zhang, Removal of phosphate anions using the modified chitosan beads: adsorption kinetic, isotherm and mechanism studies, Powder Technol., 277 (2015) 112–119.

[32] A.H. Jawad, I.A. Mohammed, A.S. Abdulhameed, Tuning of fly ash loading into chitosan-ethylene glycol diglycidyl ether composite for enhanced removal of Reactive Red 120 dye: optimization using the Box–Behnken design, J. Polym. Environ., 28 (2020) 2720–2733.

[33] A. Reghioua, D. Barkat, A.H. Jawad, A.S. Abdulhameed, A.A. Al-Kahtani, Z.A. Alothman, Parametric optimization by

[34] Box–Behnken design for synthesis of magnetic chitosan-benzil/ZnO/Fe_3O_4 nanocomposite and textile dye removal, J. Environ. Chem. Eng., 9 (2021) 105166, doi: 10.1016/j.jece.2021.105166.

[34] A.S. Abdulhameed, A.T. Mohammad, A.H. Jawad, Modeling and mechanism of Reactive orange 16 dye adsorption by chitosan-glyoxal/TiO_2 nanocomposite: application of response surface methodology, Desal. Water Treat., 164 (2019) 346–360.

[35] Y.G. Abou El-Reash, M. Otto, I.M. Kenawy, A.M. Ouf, Adsorption of Cr(VI) and As(V) ions by modified magnetic chitosan chelating resin, Int. J. Biol. Macromol., 49 (2011) 513–522.

[36] S.K. Lagergren, About the theory of so-called adsorption of soluble substances, Sven. Vetenskapsakad. Handingarl, 24 (1898) 1–39.

[37] G. Blanchard, M. Maunaye, G. Martin, Removal of heavy metals from waters by means of natural zeolites, Water Res., 18 (1984) 1501–1507.

[38] I. Langmuir, The adsorption of gases on plane surfaces of glass, mica and platinum, J. Am. Chem. Soc., 40 (1918) 1361–1403.

[39] H. Freundlich, Über die adsorption in lösungen, Zeitschrift für physikalische Chemie, 57 (1907) 385–470.

[40] W. Phasuphan, N. Praphairaksit, A. Imyim, Removal of ibuprofen, diclofenac, and naproxen from water using chitosan-modified waste tire crumb rubber, J. Mol. Liq., 294 (2019) 111554, doi: 10.1016/j.molliq.2019.111554.

[41] A. Reghioua, D. Barkat, A.H. Jawad, A.S. Abdulhameed, S. Rangabhashiyam, M.R. Khan, Z.A. Alothman, Magnetic chitosan-glutaraldehyde/zinc oxide/Fe_3O_4 nanocomposite: optimization and adsorptive mechanism of Remazol Brilliant Blue R dye removal, J. Polym. Environ., 29 (2021) 3932–3947.

[42] S. Subramaniam, K.Y. Foo, E.N. Md Yusof, A.H. Jawad, L.D. Wilson, S. Sabar, Hydrothermal synthesis of phosphorylated chitosan and its adsorption performance towards Acid Red 88 dye, Int. J. Biol. Macromol., 193 (2021) 1716–1726.

[43] A. Hofmann, M. Pelletier, L. Michot, A. Stradner, P. Schurtenberger, R. Kretzschmar, Characterization of the pores in hydrous ferric oxide aggregates formed by freezing and thawing, J. Colloid Interface Sci., 271 (2004) 163–173.

[44] H. Yan, H. Yang, A. Li, R. Cheng, pH-tunable surface charge of chitosan/graphene oxide composite adsorbent for efficient removal of multiple pollutants from water, Chem. Eng. J., 284 (2016) 1397–1405.

[45] Z. Khan, Chitosan capped Au@Pd@Ag trimetallic nanoparticles: synthesis, stability, capping action and adsorbing activities, Int. J. Biol. Macromol., 153 (2020) 545–560.

[46] S. Kumar, J. Koh, H. Kim, M.K. Gupta, P.K. Dutta, A new chitosan–thymine conjugate: synthesis, characterization and biological activity, Int. J. Biol. Macromol., 50 (2012) 493–502.

[47] A.H. Jawad, A.S. Abdulhameed, E. Kashi, Z.M. Yaseen, Z.A. Alothman, M.R. Khan, Cross-linked chitosan-glyoxal/kaolin clay composite: parametric optimization for color removal and COD reduction of Remazol Brilliant Blue R dye, J. Polym. Environ., 30 (2022) 164–178.

[48] N.N.A. Malek, A.H. Jawad, K. Ismail, R. Razuan, Z.A. Alothman, Fly ash modified magnetic chitosan-polyvinyl alcohol blend for reactive orange 16 dye removal: adsorption parametric optimization, Int. J. Biol. Macromol., 189 (2021) 464–476.

[49] H. Antony, S. Peulon, L. Legrand, A. Chaussé, Electrochemical synthesis of lepidocrocite thin films on gold substrate—EQCM, IRRAS, SEM and XRD study, Electrochim. Acta, 50 (2004) 1015–1021.

[50] S. Kang, B. Xing, Adsorption of dicarboxylic acids by clay minerals as examined by in situ ATR-FTIR and ex situ DRIFT, Langmuir, 23 (2007) 7024–7031.

[51] W. Chen, X. Zhang, Y. Zhang, M. Mamadiev, Facile and efficient synthesis of polyacrylonitrile-based functional fibers and its sorption properties of perfluorooctane sulfonate and perfluorooctanoate, J. Mol. Liq., 241 (2017) 1013–1022.

[52] M. Skulinova, C. Lefebvre, P. Sobron, E. Eshelman, M. Daly, J.F. Gravel, J.F. Cormier, F. Châteauneuf, G. Slater, W. Zheng, A. Koujelev, R. Léveillé, Time-resolved stand-off UV-Raman spectroscopy for planetary exploration, Planet. Space Sci., 92 (2014) 88–100.

[53] M. Hassan, Y. Liu, R. Naidu, J. Du, F. Qi, Adsorption of perfluorooctane sulfonate (PFOS) onto metal oxides modified biochar, Environ. Technol. Innovation, 19 (2020) 100816, doi: 10.1016/j.eti.2020.100816.

[54] W. Guo, S. Huo, J. Feng, X. Lu, Adsorption of perfluorooctane sulfonate (PFOS) on corn straw-derived biochar prepared at different pyrolytic temperatures, J. Taiwan Inst. Chem. Eng., 78 (2017) 265–271.

[55] Q. Zhang, S. Deng, G. Yu, J. Huang, Removal of perfluorooctane sulfonate from aqueous solution by crosslinked chitosan beads: sorption kinetics and uptake mechanism, Bioresour. Technol., 102 (2011) 2265–2271.

[56] Y. Su, H. Cui, Q. Li, S. Gao, J.K. Shang, Strong adsorption of phosphate by amorphous zirconium oxide nanoparticles, Water Res., 47 (2013) 5018–5026.

[57] S. Deng, G. Yu, S. Xie, Q. Yu, J. Huang, Y. Kuwaki, M. Iseki, Enhanced adsorption of arsenate on the aminated fibers: sorption behavior and uptake mechanism, Langmuir, 24 (2008) 10961–10967.

[58] Q. Hu, H. Liu, Z. Zhang, Y. Xie, Nitrate removal from aqueous solution using polyaniline modified activated carbon: optimization and characterization, J. Mol. Liq., 309 (2020) 113057, doi: 10.1016/j.molliq.2020.113057.

[59] S.S. Elanchezhiyan, S. Muthu Prabhu, J. Han, Y.M. Kim, Y. Yoon, C.M. Park, Synthesis and characterization of novel magnetic Zr-MnFe$_2$O$_4$@rGO nanohybrid for efficient removal of PFOA and PFOS from aqueous solutions, Appl. Surf. Sci., 528 (2020) 146579, doi: 10.1016/j.apsusc.2020.146579.

[60] C.Y. Tang, Q. Shiang Fu, D. Gao, C.S. Criddle, J.O. Leckie, Effect of solution chemistry on the adsorption of perfluorooctane sulfonate onto mineral surfaces, Water Res., 44 (2010) 2654–2662.

[61] F. Wang, K. Shih, Adsorption of perfluorooctanesulfonate (PFOS) and perfluorooctanoate (PFOA) on alumina: influence of solution pH and cations, Water Res., 45 (2011) 2925–2930.

[62] G. Liu, L. Liao, Z. Dai, Q. Qi, J. Wu, L.Q. Ma, C. Tang, J. Xu, Organic adsorbents modified with citric acid and Fe$_3$O$_4$ enhance the removal of Cd and Pb in contaminated solutions, Chem. Eng. J., 395 (2020) 125108, doi: 10.1016/j.cej.2020.125108.

[63] S. Fan, J. Tang, Y. Wang, H. Li, H. Zhang, J. Tang, Z. Wang, X. Li, Biochar prepared from co-pyrolysis of municipal sewage sludge and tea waste for the adsorption of methylene blue from aqueous solutions: kinetics, isotherm, thermodynamic and mechanism, J. Mol. Liq., 220 (2016) 432–441.